RSC Advances

ROYAL SOCIETY OF CHEMISTRY

www.rsc.org/advances

Journal Name

ARTICLE

Enhanced Nonlinear Optical Properties of Silver-Graphene Oxide Nanocomposite Measured by Z-Scan Technique

****

S Biswas,[a] A K Kole,[a] C S Tiwary,[b] and P Kumbhakar[a]*

Nonlinear optical properties (NLO) of the graphene oxide-silver (GO-Ag) nanocomposite has been investigated by the Z-Scan setup at Q-switched Nd:YAG laser second harmonic radiation i.e., at 532nm excitation in nanosecond regime. A noteworthy enhancement in the NLO properties in GO-Ag nanocomposite has been reported in comparison with those of the synthesized GO nanosheet. The extracted value of third order nonlinear susceptibility (χ_3), at a peak intensity of I_0 = 0.2 GW/cm^2, for GO-Ag has been found out to be 2.8 times larger than that of GO. The enhancement in NLO properties in GO-Ag nanocomposite may be attributed to the complex energy band structures formed during the synthesis which promote resonant transition to the conduction band via surface Plasmon resonance (SPR) at low laser intensities and excited state transition (ESA) to the conduction band of GO at higher intensities. Along with it photogenerated charge carriers in the conduction band of silver or the increase in defect states during the formation of GO-Ag nanocomposite may contribute to ESA. Open aperture Z-scan measurement indicates reverse saturable absorption (RSA) behavior of the synthesized nanocomposite which is a clear indication of the optical limiting (OL) ability of the nanocomposite.

1. Introduction

Recently, noble metal nanocomposite with low dimensional materials like graphene oxide (GO) has attracted much attention due to its enhanced linear and nonlinear optical (NLO) properties [1-4]. Unlike graphene which have sp^2 hybridized Π conjugated carbon [5, 6] GO has both sp^2 and sp^3 carbon domains [7-9] and due to the presence of oxygen containing group it is hydrophilic in nature and thus it gets dissolves into water readily. The band gap of GO can be tuned successfully over a wide spectral range by adjusting the ratio of sp^2 and sp^3 carbon atoms. Also due to the presence of hydroxyl (OH−) and epoxy (–COO−) groups at the basal plane and carboxyl groups (–COO−) at the edge of the molecular structure, GO can interact with varied organic and inorganic materials [10-12]. Due to these advantageous properties, GO composites are used in wide varieties of applications, such as in drug delivery [13], magnetic resonance imaging [14], and memory devices [15], as super capacitors [16], optoelectronic devices [17], and optical limiting devices and for designing optical switches [18]. However, for later applications it is desirable that the used materials will have large NLO properties. In earlier reports authors have demonstrated NLO properties of GO in suspension, such as both saturable (SA) [19] and reverse saturable absorption (RSA) [20] properties have been reported in GO suspension. In some reports, at low intensity SA, at higher intensities two photon absorption (2PA) [21] and excited state absorption (ESA) [22] have been demonstrated in GO. Wang *et al.* [18] have demonstrated broad band optical limiting properties of graphene dispersed in organic solvent by using Z-Scan technique both at 532nm and 1064nm wavelengths. Nalla *et al.* [23] has reported a large nonlinear absorption and nonlinear refraction coefficients of a conjugated polymer–GO composite in nanosecond regime. NLO and optical limiting (OL)

[a] Nanoscience Laboratory, Dept. of Physics, National Institute of Technology Durgapur, 713209West Bengal, India
[b] Department of Material Engineering, Indian Institute of Science, Bangalore-560012, India

properties of graphene families like GO-nanosheets, graphene nanosheets, GO-nanoribbons and graphene nanoribbons have also been reported [24]. Interaction of metal nanoparticles with graphene has been examined by Subrahmanyamm *et al.* [25]. Kalanoor *et al*. [26] have investigated NLO properties of silver decorated graphene in picoseconds region by Z-scan method under 1064nm excitation and they have observed that the synthesized material exhibited SA behavior under the incidence of low intensity but it show RSA behavior at higher intensity of the incident laser radiation. Sadrolhosseini *et al.* [27] have investigated NLO properties of the Gold and GO nanocomposite, synthesized by laser ablation technique, by the Z-Scan technique. However, the NLO properties of GO-Ag nanocomposite at the near resonant excitation wavelength of 532nm have been studied very sparingly by using Z-Scan technique.

In this work, we have reported the enhanced NLO property of a chemically synthesized GO-Ag composites in comparison with that of GO in suspension using Z-Scan technique at a pump wavelength of 532nm. Open aperture (OA) Z-Scan measurement has revealed that the 2PA coefficient of GO-Ag composites is 45.4 GW/cm^2 at peak intensity of I_0 = 0.2 GW/cm^2 which is ~2.7 times larger than that of GO measured at the same intensity. Third order nonlinear susceptibility of the materials has been found to be 5.7×10^{-12} esu which is also 2.8 times larger than the value obtained for GO. A mechanism using an energy band diagram of the nanocomposite has been proposed to explain the observed enhancement in NLO properties. The enhancement in NLO properties has been attributed to the complex energy band structures formed during the synthesis of nanocomposite which promote resonant transition via surface Plasmon resonance (SPR) at low laser intensities and excited state transition (ESA) conduction band of GO at higher intensities. Also photo-generated charge carriers in the conduction bands of silver or the increase in defect states during the formation of GO-Ag nanocomposite may contribute to ESA.

2. Experiments

In this work, GO has been synthesized by using modified Hummers' method [28]. However, the synthesis technique of GO is described below, briefly. At first 3gm of graphite powder has been collected by scratching pure graphite flakes and then added to the mixture of 360 ml H_2SO_4 and 40 ml H_3PO_4. Then the system is transferred to an ice bath and 18gm of $KMnO_4$ is added drop-wise in 30 min and the mixture is stirred for 12 hour. After that 3ml of H_2O_2 (30%) has been added to the solution with simultaneous addition of the 400gm ice. After that we allow the system to settle down and discarded the supernatant. The obtained solid remnants is further washed with 200ml of distilled water, 200ml of 30% HCl and then with 200ml (90%) ethanol. Finally the product is filtered and dried at room temperature to get GO. Further, GO-Ag nanocomposite has been prepared by solvothermal technique. And for preparing GO-Ag nanocomposite, at first we have synthesized Ag nanoparticles by chemical technique and by reducing 2mM of silver nitrate ($AgNO_3$) with the help of 2mM freshly prepared solution of sodium boro-hydrade ($NaBH_4$) at room temperature. The freshly prepared Ag-sol is mixed with 200mg of GO dispersed in water and the then the mixture is magnetically stirred for half an hour. After that total solution has been transferred into a stainless steel autoclave where it has been kept at 170°C temperature for 8h. Final solution is collected and centrifuged at 10000 rpm and washed several times with DI water. The remnant is then collected in a Petri dish and left for drying at room temperature.

Further, the dried sample is re-dispersed in DI water whenever required for characterizations and for measurement of optical properties. UV-Vis absorption characteristics of the sample have been measured by using a double-beam UV-Vis spectrophotometer (Hitachi U-3010). X-ray diffraction (XRD) pattern has been recorded in an X'Pert PRO diffractometer, Pan Analytical make with Cu K_α target with a step size of 0.002°. TEM and HRTEM images of the samples have been collected in a JEOL 2100 TEM.

The NLO properties of the sample have been measured by *Z*-scan technique, [29] the details of which are described elsewhere. [30] However, some useful parameters of the Z-scan measurement are given below. Two different techniques, namely open aperture (OA) and closed aperture (CA) have been used for the determination of the NLO properties of the samples. A Q-switched Nd:YAG laser at 532 nm radiation with 10 ns pulse duration with variable peak intensity have been used to measure OA and CA *Z*-Scan transmission traces at room temperature. A converging lens of focal length 21.6 cm is used to focus the transmitted laser beam. The beam waist (w_0) and the confocal parameter (z_0) at the focus are 36.6 μm and 8 mm, respectively. A quartz cuvette of path length (L) 2 mm is used and so the "thin sample" approximation, $L<z_0$, is satisfied comfortably. The cuvette is mounted in a translation stage which can translate the sample in the pre-focal and post-focal directions along the direction of propagation (z-axis) of the transmitted laser beam.

3. Results and discussion

3.1 Characterizations of the GO and GO-Ag nanocomposite

UV-Vis absorption spectra of the GO and GO-Ag dispersed in DI water has been taken in the spectral region of 200-800nm and is presented in Figure 1a. GO is characterized by the presence of a prominent single peak at ~225nm due to the Π- Π* transition [31] in aromatic C-C bond, whereas GO-Ag nanocomposite exhibits two peaks, one at 236nm and another at 410nm. The first peak is again due to Π- Π* transition in aromatic C-C bond of GO but a red shift of 11nm is observed which is assigned to restoration of charge conjugation [1] in GO sheet. The simultaneous appearances of peaks due to both GO and Ag in the absorption spectra is a clear indication of the formation of GO-Ag nanocomposite.

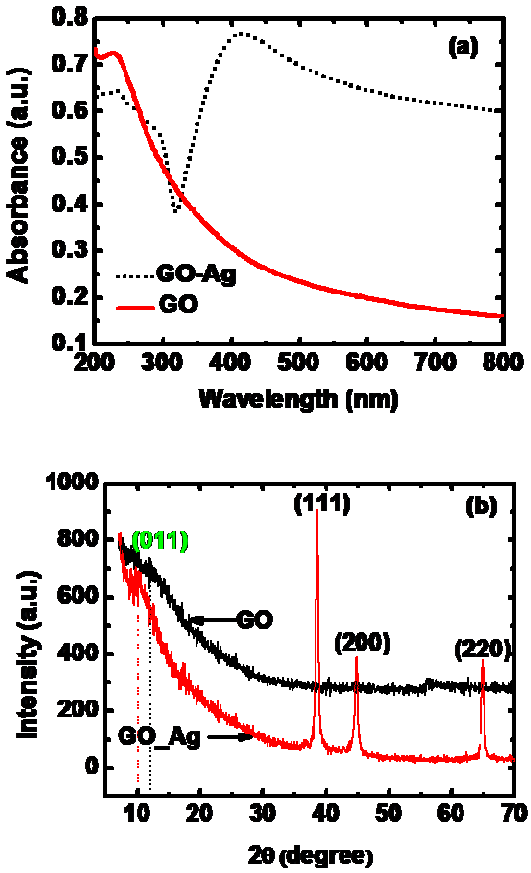

Fig. 1 (a) UV-Vis absorption spectra of the GO (solid line) and GO-Ag (dotted line) composites. (b) XRD pattern of the GO and GO-Ag composites.

Figure 1b shows the XRD patterns of both the samples. In the XRD pattern of GO, a week peak at ~ 12° appeared due to reflection from (*001*) [32], having basal plane interplanner spacing d_{001} of 0.736 nm. In case of GO-Ag nanocomposite the XRD peak due to (*001*) of GO has been shifted to 10° and the corresponding basal plane interplannar spacing is 0.883 nm. The observed increment in the interlayer spacing of GO may is ascribed to the insertion of silver nanoparticles within the GO layers. The sharp peaks at 38.6°, 44.8° and 64.8° are originated due to the reflection from (*111*), (*200*) and (*220*) crystallographic planes of face centered cubic (fcc) structure [33] of the silver nanoparticles. The average crystallite size of silver nanoparticles is extracted to be 23 nm, from XRD pattern by using Debye-Scherrer [34] equation.

For structural study we have performed transmission electron microscopy (TEM) analysis and for that the synthesized GO-Ag nanocomposite has been dispersed in de-ionized water and a drop of the solution is deposited over the carbon coated copper grid and dried it before observation in TEM. The inset at the right bottom of the Figure 2a depicts the particle size distribution of silver nanoparticles (measured from several bright field images taken at different portion of the grid) and the average value of particle size is measured to be 30nm. The high resolution TEM (HR-TEM) image of the GO-Ag composite sheet is shown in Figure 2b and it has provided a deep insight about the crystallinity and microstructure of the silver and as well as GO. The portion marked as A in the HRTEM image has been identified as the crystallographic planes of silver as the distance between the crystallographic planes of section A extracted to be 0.231nm and can be easily identified as (111) plane [35] of the silver nanoparticles. The presence of (111) crystallographic plane of silver in GO-Ag nanocomposites is also identified in XRD analysis.The magnified portion of the section A has been shown as inset at right top and the corresponding fast Fourier transform (FFT) pattern is shown at the left top of the figure which shows the closed packed hexagonal lattice. The clear and regular lattice fringes in FFT pattern of the section A have confirmed that the silver nanoparticles embedded on it are highly crystallized. The single hexagonal pattern in FFT images indicates that the silver nanoparticles are formed by with the crystalline facet (*111*).

Similarly the enlarged portion of section B identifies as the crystallographic plane of GO which is presented as inset at right bottom and the corresponding FFT is shown in left bottom of the Figure 2b. The regular hexagonal pattern of sp^2 hybridized matrix [36, 37] of GO can be easily identified in the enlarged portion of section B. The average value of in plane C-C spacing has been evaluated from HRTEM image and it is found to be 0.16 nm which very close to the literature value of C-C spacing of 0.152 nm [37] for graphite which also indicates that like grapheme, here also carbon atoms are sp^2 hybridized and arranged in planer arrangement in GO. We have taken the FFT images of several portions of the HRTEM images and it is observed that hexagonal pattern is repeated in all over the crystallographic plane of GO. However a close observation over a large portion has revealed some irregularities in the hexagonal pattern which is due to the presence of the oxygen containing group in the GO. It has been reported earlier [38, 39] that irregularities in graphene crystallographic plane may be due to the amorphous carbon adsorbed on it and it is referred to as adventitious [40] carbon or may be due to the oxidized carbon formed during the preparation of GO by Hummers method.

3.2 *Z*-scan measurements

Open aperture (OA) *Z*-scan measurement have been performed to reveal the different mechanisms, like multi-photon absorption (MPA) [41], excited state absorption (ESA) [22] responsible for nonlinear absorption (NLA) in the synthesized materials. In Figure 3a we have presented the intensity dependent OA *Z*-Scan data for GO. Small circles represent OA *Z*-scan transmission traces and the solid lines are the theoretical fitting using the equation [41],

$$T_{nPA}(Z) = 1 - \beta_{nPA} I_0^{n-1} L_{eff}^{(n)} n^{-\frac{3}{2}} \left(1 + \frac{Z^2}{Z_0^2}\right)^{-(n-1)} \quad . \qquad (1)$$

Where n = 2, 3, 4….etc. for two, three or four photon absorption and β_{nPA} is the n-photon absorption coefficient, I_0 is the intensity at the focus, L_{eff} is the effective path length and Z_0 is the Rayleigh range. From the figure it is evident that normalized transmission decreases as the sample move towards the focus and forms a valley with a deep at the focus. The deep at the focus increases with the increasing intensity indicating the presence of reverse saturable absorption (RSA) in GO. In case of organic materials both ESA and 2PA is the

dominant process leading to the nonlinear absorption, but for non-resonant transition, like in the present case where the wavelength of the excited laser (532 nm) is far away from the UV-vis absorption peak of the GO (225 nm), 2PA is the dominant NLA process. We have fitted the OA *Z*-scan traces of GO for different intensities using the simulated curve of 2PA by using Eq (1).

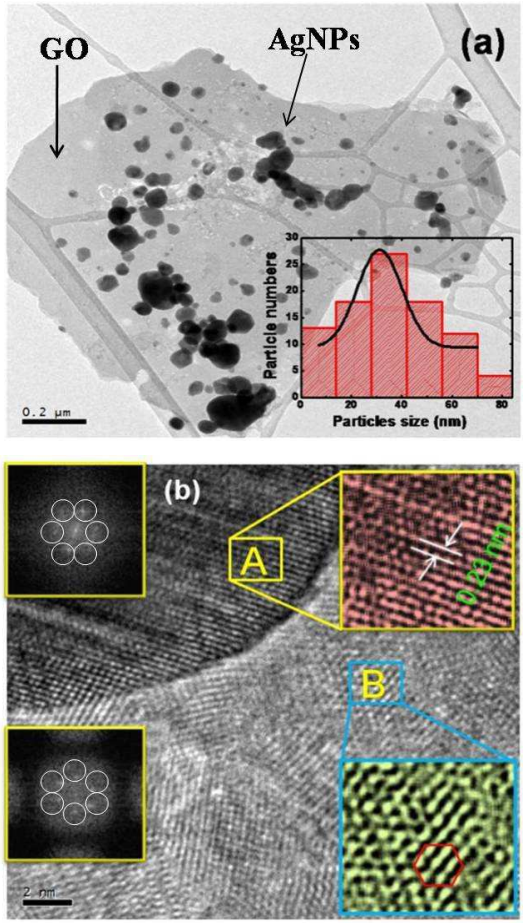

Fig. 2 (a) TEM image of GO-Ag composites.(b) High resolution TEM image of the crystallographic planes of GO-Ag where enlarge portion of the section A ((111) planes of silver nanoparticles) and enlarged portion of section B (hexagonal crystal planes of the sp^2 matrix of GO) is shown in the right top and right bottom. The corresponding FFT (Fast Fourier Transform) image of the section A and B are shown in left top and left bottom of the figure.

The extracted values of β_{2PA} for different intensities are presented in the Table 1 and it is evident that the value of β_{2PA} increases with increasing intensity so along with 2PA, ESA may contribute to NLA in GO. The highest extracted value of β_{2PA} of our synthesized GO is found out to be 17 cm/GW which is comparable with that of GO sheets suspended in Di-methyl formamide, as reported by Zhang *et al.* [42] in nanosecond regime at 532nm excitation. Kalanoor *et al.* [26] has reported β_{2PA} value of 34±3 cm/GW of functionalized graphene in nanosecond regime at 532 nm laser excitation. Liu *et al.* [43] has investigated the NLO properties of GO in nanosecond as well as picoseconds regime at 532nm laser excitation. We have also reported intensity dependent enhancement of β_{2PA} value as also observed in our experiment.

OA Z-scan experiments with GO-Ag nanocomposite have been performed and the results are presented in Figure 3b. It is also found to exhibit RSA behaviour, like GO, and the Z-scan dip at the focus increases with increasing intensity. We have fitted the OA *Z*-Scan traces presented by solid spheres in the figure with the theoretical simulation using Eq. (1). From the theoretical fittings, β_{2PA} have been extracted for different intensities and the results are summarized in Table 1. From the Table 1, it can be seen that a noteworthy increment (2.7 times) in β_{2PA} value in GO-Ag nanocomposite in comparison to that of GO has been occurred. The observed β_{2PA} value of GO-Ag nanocomposite is very close to that of

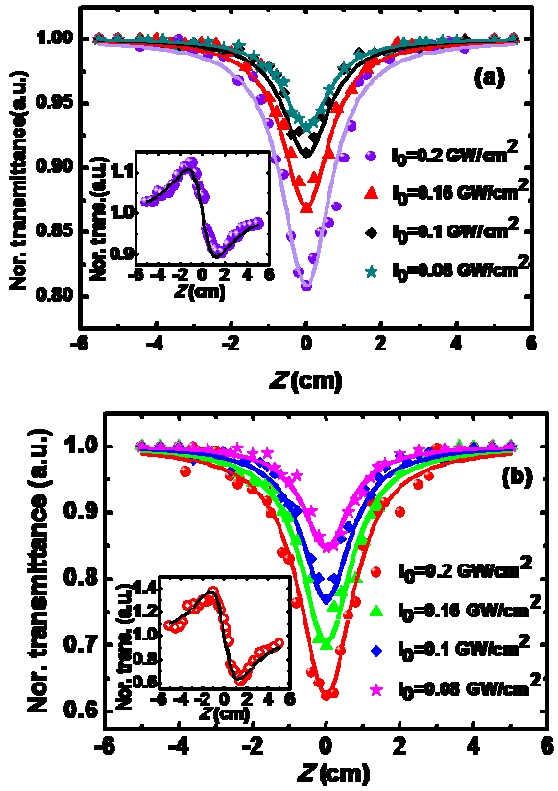

Fig. 3 (a) Intensity dependent OA *Z*-scan curve (scattered points are the experimental points and solid lines are 2PA theoretical fitting) of the GO and inset at right bottom shows the CA Z-scan plot of GO at an intensity of 0.2 GW/cm^2 (scattered points are experimental points and solid line is the theoretical fitting). (b) Intensity dependent OA *Z*-scan curve (scattered points are the experimental points and solid lines are 2PA theoretical fitting) of the GO-Ag and inset at right bottom shows the CA Z-scan plot of GO at an intensity of 0.2 GW/cm^2 (scattered points are experimental points and solid line is the theoretical fitting).

earlier reported value of 46 cm/GW of Au-graphene nanocomposite [44] in nanosecond regime at 532nm. Chantharasupawong *et al.* [10] has also investigated NLO properties of GO, fluorinated grapheneoxide (F-GO) and highly fluorinated graphene oxide (HF-GO) in nanosecond regime by 532 nm laser exciatation. However, their obtained β_{2PA} values are 0.9 cm/GW for F−GO, 0.45 cm/GW for HFGO, and 0.2 cm/GW for GO, which are found to be much lower than that obtained in our synthesized GO-Ag nanocomposite.

Table 1 The extracted values of $\beta_{2PA,}$ n_2 and χ_3 of GO and GO-Ag nanocomposite at different laser intensities.

NLO parameters	GO	GO-Ag
β_{2PA} (cm/GW) at I_0=0.2 GW/cm^2	17	45.4
β_{2PA} (cm/GW) at I_0=0.16 GW/cm^2	13.5	39.7
β_{2PA} (cm/GW) at I_0=0.1 GW/cm^2	12	32.4
β_{2PA} (cm/GW) at I_0=0.08 GW/cm^2	10.8	30
n_2 (cm^2/W)	1.2×10^{-13}	5.7×10^{-12}
χ_3 (esu)	5.7×10^{-12}	16×10^{-12}

The observed increment in NLA can be explained in terms of the energy band diagram of GO-Ag composites, which has been depicted in Figure 4a. GO contains sp^2 matrix of graphene and sp^3 matrix of oxygen containing group while silver nanoparticles generally attached to it through oxygen containing group. Energy band gap in sp^2 matrix is low and is responsible for saturable absorption due to bleaching of valance band at low intensity while energy band gap of sp^3 matrix is large and at large intensities of used laser beam electrons in the valance band pumped to conduction band by 2PA and become free carriers. In our case during the formation of the GO-Ag nanocomposite the energy levels of GO and silver nanoparticles interact and may form a complex energy levels as shown in the Figure 4a.

Subrahmanyam *et al.*[25] from the first-principle calculation has shown that there are intermediate energy states of metal which extends up to the conduction band of graphene in case of metal graphene nanocomposite. In our case, the linear absorbance peak of silver nanoparticles is occurred at ~410 nm due to SPR, so when the GO-Ag nanocomposite sample is irradiated with the laser radiation of wavelength 532 nm being close to the SPR wavelength, a near resonant 2PA transition may occur. These excited electrons may be transferred to the GO conduction band as metal energy level extends up to GO conduction band and promotes the ESA at higher laser intensities. Moreover, absorption associated with photo-generated charge carriers in the conduction bands of silver may also leads to ESA or the increase in defect states during the formation of GO-Ag nanocomposite might also contribute to ESA and thus the enhancement in NLA has been taken place in GO-Ag nanocomposite in comparison with that of GO.

To find out the nonlinear refraction (NLR) coefficient (n_2) we have performed the closed aperture *Z*-scan measurement and the *Z*-scan traces are depicted in the inset of Figure 3a. The black spheres are the experimental points and the solid line (Green) is the theoretical simulation by using the relation as proposed by Guo *et al.* [45] where pure NLR can be obtained from the following equation,

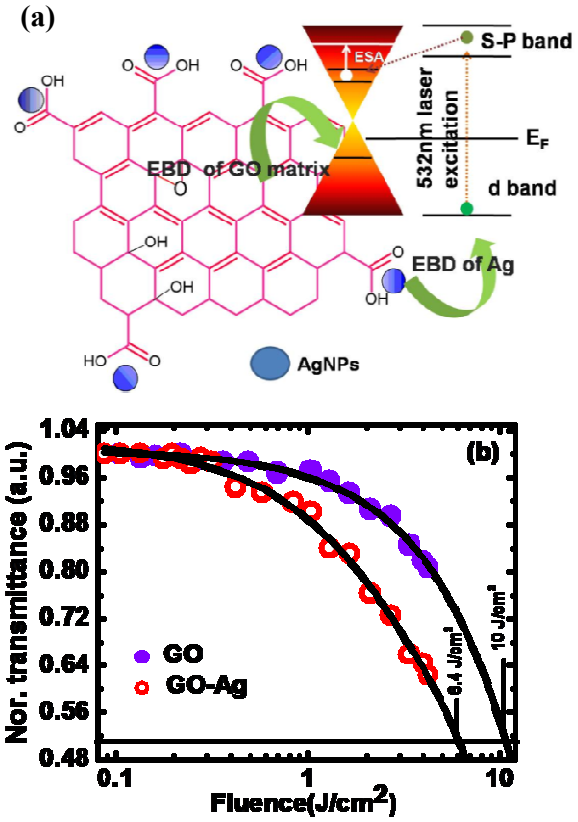

Fig. 4 (a) Energy band diagram (EBD) of the GO-Ag composites depicts the electron transfer mechanism in GO-Ag composites under laser illumination. (b) Optical limiting property of GO and GO-Ag nanocomposite.

$$T_{th-refr}(Z) = 1 + \frac{(1-s)^{\mu}\sin\xi}{s(1+x^2)}\Delta\phi_0 . \quad (2)$$

Where s is linear transmittance and

$$T_{th-ref}(Z) = \frac{T_{CA}(Z)}{[T_{OA}(Z)]^p} . \quad (3)$$

Where, $x = Z/Z_0$, $p = 1+0.63(1-s)^2$, $\xi = -\frac{4x\ln(1-s)}{(x^2+9)}$. The peak valley difference in transmittance (ΔT_{p-v}) of the CA Z-scan trace can be associated to $|\Delta\phi_0|$ [44] by the following relation,

$$\Delta T_{p-v} \cong 0.406[1-\sum_{m=1}^{6} a_m\{1-(1-s)^{0.67}\}^m]|\Delta\phi_0| \quad (4)$$

Where, $a_1 = -0.4070$, $a_2 = -0.1461$, $a_3 = -0.4841$, $a_4 = 0.3862$, $a_5 = 0.0423$, and $a_6 = -0.3696$. For calculating the NLR coefficient of the samples at first CA Z–scan traces are collected experimentally by using an aperture with known transmittance s. Then we have calculated $T_{th\text{-}ref}(Z)$ at different values of Z by using Eq. (3). Then from the measured value of ΔT_{p-v} of GO nanosheets as shown in Figure 3a, $\Delta\phi_o$ is calculated by using Eq. (4), and then n_2 is calculated by using the relation $\Delta\phi_o = 2\pi n_2 I_o L_{eff}/\lambda$ and the extracted value is 1.2×10^{-13}cm^2/GW. Further, the nature of CA *Z*-scan curve indicates the self-focusing property of the materials.[29,30]

Different mechanisms have been proposed to describe the observed NLR of GO in suspension. The electronic polarization, molecular reorientation effect, nonlinear scattering, excited state refraction, free carrier refraction, and thermal effect are most common reason for observed NLR [42]. To determine the effect of thermal nonlinearity present in our system we have calculated the acoustic buildup time [46] which is the time required to propagate the sound wave generated due to the motion of the laser through the medium across the beam radius and is given by [46]

$$\tau_{ac} = \omega_0/V_s \quad (5)$$

Where, ω_0 beam waist radius and V_s is the velocity of propagation of sound wave in the medium. In the present case, the extracted value of the τ_{ac} is 24.6 ns which is greater than the laser pulse width thus thermal nonlinearity is absent in the present experiment. In femtosecond time region free carrier refraction, excited state refraction and electronic polarization [42, 47] contributions contribute to NLR, whereas in picoseconds region in addition to these Π electrons and bound electrons in valance band and free electrons in conduction band [42] contribute to NLR. It has been reported that in nanosecond regime, reorientation and alignment of GO sheets in solution and transient thermal effect [42] comes into play. As we have shown earlier that the thermally induces nonlinearity is absent in the present case thus observed NLR of GO in dispersion may be attributed to the reorientation and alignment of GO sheets in the solution.

We have also further performed the CA *Z*-scan experiment in the GO-Ag nanocomposite at the highest intensity used in OA experiment and the result is presented in the inset of Figure 3b and by following the analytical procedure as described earlier, the extracted value of n_2 and χ^3 are 4.5×10^{-13} cm^2/GW and 16×10^{-12} e.s.u., respectively. Thus we have observed 2.8 times increase in third order nonlinear susceptibility in GO-Ag nanocomposite in comparison with that of GO. Observed enhancement in NLR may be due to the decoration of metal nanoparticles of average size of 30nm and some are greater than 100nm on the sheets of GO which acts as new scattering centre. The observed value of the χ^3 of GO-Ag nanocomposite can be compared with χ^3 value of graphene-zinc porphyrin, and graphene-copper porphyrin composites measured by Krishna *et al.* [48] at nanosecond regime by Nd:YAG laser at 532nm laser excitation. The reported value of χ^3 of graphene-zinc porphyrin, and graphene-copper porphyrin composites are 7.1×10^{-12} and 8.5×10^{-12} e.s.u., respectively. Zhu *et al.* [49] has reported similar value of imaginary third-order susceptibility [Im (χ^3) ~ 17.62 ± 4.03×10^{-12} e.s.u.] of GO covalently functionalized with zinc phthalocyanine (PcZn), GO–PcZn at nanosecond regime and 532nm excitation by Nd:YAG laser.

Further it has been found that the synthesized materials are demonstrating optical limiting (OL) property. OL properties of nanocomposite of GO with Au, Pd, etc. have been reported earlier [50] but the OL property of GO-Ag nanocompsite has not been studied, so far. In Figure 4b the variations of sample transmission with input laser fluence for both GO and GO-Ag nanocomposite have been depicted by taking the data from the corresponding OA Z-scan traces. The position dependent fluence can be evaluated from the Eq. (6),

$$F_{in} = \frac{4\sqrt{\pi \ln 2}E_0}{\pi^2\omega_0^2\left(1+\frac{z^2}{z_0^2}\right)}. \quad (6)$$

Where, F_{in} is the input laser fluence, E_0 is the used laser energy and ω_0 laser beam radius at the focus. It is clearly evident from the Figure 4b that the materials show a promising OL activity. The OL threshold, which is defined as the input laser fluence for which the transmittance of the sample is 50%, is slightly better in GO-Ag nanocomposite (6.4 J/cm^2) than that of GO (10 J/cm^2). The improved OL effect in GO-Ag may attribute to the increase in scattering centres, ESA at higher intensity in GO-Ag due to the presence of metals nanoparticles in the GO sheets.

4. Conclusions

Here, we have presented the observation of enhanced two-photon absorption properties of GO-Ag nanocomposite in comparison to those of GO under the excitation of a ns pulsed visible laser radiation of 532 nm wavelength, which has rarely been reported earlier. The NLO properties have been measured by OA and CA Z-scan techniques at a visible wavelength of 532 nm, which is obtained by second harmonic generation of a Q-switched Nd:YAG laser fundamental wavelength of 1064 nm. GO have been synthesized by modified Hummers method and then GO-Ag nanocomposite has been synthesized by simple hydrothermal method. The beautiful decoration of silver nanoparticles on GO sheets has been confirmed by analysing the linear absorption characteristic, XRD data and transmission electron microscopy. Intensity dependent OA measurement shows that the extracted values of β_{2PA} of GO is 17 cm/GW whereas for GO-Ag is 45.4 cm/GW at a highest intensity 0.2 GM/cm^2 used in the experiment. Thus a clear 2.6 times enhancement

in β_{2PA} value is observed in GO-Ag nanocomposite in comparison with GO. To explain the mechanism for enhancement in NLO properties of GO-Ag nanocomposite, an energy band diagram have been proposed, where ESA along with 2PA may contribute in observed enhancement in β_{2PA} value. The effect of thermally induced nonlinearity in NLR has been investigated and result shows that the effect can be neglected in the present case. Extracted value of third order nonlinear susceptibility (χ_3) at a peak intensity of I_0 = 0.2 GW/cm^2 for GO-Ag has been found out to be 2.8 times larger than that of GO. OL activity of the synthesized materials has been investigated and GO-Ag nanocomposite shows better OL threshold than that of GO. Thus the synthesized GO-Ag nanocomposite might be a promising NLO material with improved OL effect and can safely be used as good optical limiter in different military, medical operations.

Acknowledgements

Authors are grateful to CSIR, Govt of India for the grant CSIR No. 03(1328)/14/EMR-II and TEQIP-II, NIT Durgapur, Govt. of India for the partial financial supports. Also the partial financial support from UGC, NRCM, IISc Bangalore is acknowledged. Authors are also grateful to Prof. U. Chatterjee, Dept. of Physics, Burdwan University, Burdwan for his permission to use some of the experimental facilities available in his laboratory.

References

1 D. Li, and R. B. Kaner, *Science.* 2008, **320**, 1170.

2 Z. Liu, Q. Liu, Y. Huang, Y. Ma , S. Yin, X. Zhang, W. Sun and Y. Chen, *Adv. Mater*., 2008, **20**, 3924.

3 A. K. Geim, and K. S. Novoselov, *Nat. Mater*., 2007, **6**, 183.

4 D. Yu, Y. Yang, M. Durstock, J.-B Baek, and L Dai, *ACS Nano,* 2010, **4**, 5633.

5 H. Z. Yang, X. B. Feng, Q. Wang, H. Huang, W. Chen, A. T. S. Wee, and W. Ji, *Nano Lett.,* 2011, **11**, 2622.

6 Q. L. Bao, H. Zhang, Y. Wang, Z. H. Ni, Y. L. Yan, Z. X. Shen, K. P. Loh, and D. Y. Tang, *Adv. Funct. Mater*., 2009, **19,** 3077.

7 X. F. Jiang, L. Polavarapu, S. T. Neo, T. Venkatesan, and Q. H. Xu, *J. Phys. Chem. Lett*., 2012, **3**, 785.

8 Z. B. Liu, X. Zhao, X. L. Zhang, X. Q. Yan, Y. P. Wu, Y. S. Chen, and J. G. Tian, *J. Phys. Chem. Lett*., 2011, **2**, 1972.

9 O. C. Compton and S. T. Nguyen, *Small*. 2010, **6**, 711.

10 P. Chantharasupawong, R. Philip, N. T. Narayanan, P. M. Sudeep, A. Mathkar, P. M. Ajayan, J. Thomas. *J. Phys. Chem. C.,* 2012, **116**, 25955.

11 X. Zhang, X. Yang, Y. Ma, Y. Huang, and Y. Chen, *J. Nanosci. Nanotechno*., 2010, **10**, 2984.

12 X. Huang, Z. Yin, S. Wu, X. Qi, Q. He, Q. Zhang, Q. Yan, F. Boey, and H. Zhang, *small.* 2011, **7**, 1876.

13 X Sun, Z. Liu, K. Welsher, J. Robinson, A. Goodwin, S. Zaric, and H. Dai, *Nano Res*., 2008, **1**, 203.

14 X. Ma, H. Tao, K. Yang, L. Feng, L. Cheng, X. Shi, Y. Li, L. Guo, and Z. Liu, *Nano Res*., 2012, **5**, 199.

15 X.-D. Zhuang, Y. Chen, G. Liu, P.-P. Li, C.-X. Zhu, E.-T. Kang, K.-G. Noeh, B. Zhang, J.-H Zhu, and Y.-X. Li, *Adv. Mater*., 2010, **22**, 1731.

16 S. Chen, J. Zhu, X. Wu, Q. Han, and X. Wang, *ACS Nano.,* 2010, **4**, 2822.

17 Z. Liu, Q. Liu, Y. Huang, Y. Ma, S. Yin, X. Zhang, W. Sun, and Y. Chen, *Adv. Mater*., 2008, **20**, 3924.

18 B. J. Wang, Y. Hernandez, M. Lotya, J. N. Coleman, and W. J. Blau, *Adv. Mater*., 2009, **21**, 2430.

19 S. Kumar, M. Anija, N. Kamaraju, K. S. Vasu, K. S. Subrahmanyam, A. K. Sood, and C. N. R. Rao. *Appl. Phys. Lett*., 2009, **95**, 191911.

20.G.-K. Lim, Z.-L. Chen, J. Clark, R. G. S. Goh, W.-H. Ng, H.-W. Tan, R. H. Friend, P. K. H. Ho, and L.-L. Chua, *Nat. Photon.,* 2011, **5**, 554.

21 Z.-B. Liu, Y.-F. Xu, X.-Y. Zhang, X.-L. Zhang, Y.-S. Chen, and J.-G. Tian, *J. Phys. Chem. B*., 2009, **113**, 9681.

22 B. Gu, W. Ji, P. S. Patil, S. M. Dharmaprakash, and H.-T. Wang, *Appl. Phys. Lett*., 2008, **92**, 091118.

23 V. Nalla, L. Polavarapu, K. K. Manga, B.-M. Goh, K. P. Loh, Q.-H. Xu and W. Ji, *Nanotech*., 2010**, 21,** 415203.

24 M. Feng, H. Zhan, and Y. Chen, *Appl. Phys. Lett*., 2010, **96**, 033107.

25 K. S. Subrahmanyam, A. K. Manna, S. K. Pati, and C. N. R. Rao, *Chem. Phys. Lett.,* 2010**, 497**, 70.

26 B. S. Kalanoor, P. B. Bisht, S. A. Ali, T. T. Baby, and S. Ramaprabhu. *J. Opt. Soc. Am. B*., 2012, **29**, 1884.

27 A. R. Sadrolhosseini, A. S. M. Noor, N. Faraji, A. Kharazmi, M. A. Mahdi, *J. Nanomat*. **2014**, Article ID 962917.

28 W. S Hummers and R. E. Offeman, *J. Am. Chem. Soc*., 1958, **80**, 1339.

29 M. Sheik-Bahae, A. A. Said, T. H. Wei, D. J. Hagan, and E. W. Van Stryland, *IEEE J. Quantum Electron*., 1990, **26**, 760.

30 P. Kumbhakar, A. K. Kole, C. S. Tiwary, S Biswas, S Vinod, J Taha-Tijerina, U. Chatterjee, P.M. Ajayan, *Adv. Opt. Mat.*, 2015, **3**, 828.

31 Y. Zhou, Q. L. Bao, L. A. L. Tang, Y. L. Zhong, and K. P. Loh, *Chem. Mater*., 2009, **21**, 2950.

32 S. Bykkam, V. Rao. K, S. Chakra. CH and T. Thunugunta, *Int. J. Adv. Biotechnol. Res.,* 2013, **4**, 142.

33 H. Mao, J. Feng, X. Ma, C. Wu and X. Zhao, *J. Nanopart. Res*., 2012, **14**, 887.

34 T. R. Herrero, J. D. R. Blanco, E. H. Oelkers and L. G. Benning, *J. Nanopart. Res*., 2011, **13**, 4049.

35 H. Mao, J. Feng, X. Ma, C. Wu and X. Zhao, *J Nanopart Res.,* 2012, **14**, 887.

36 F. A. De La Cruz and J. M. Cowley, *Nature,* 1962, **196**, 468.

37 G. Eda, G. Fanchini and M. Chhowalla, *Nat. Nanotechnol.,* 2008, **3**, 270.

38 T. J. Booth, P. Blake, R. R. Nair, D. Jiang, E. W. Hill, U. Bangert, A. Bleloch, M. Gass, K. S. Novoselov, M. I. Katsnelson, A. K. Geim, *Nano Lett.*2008., **8**, 2442.

39 J. C. Meyer, C. Kisielowski, R. Erni, M. D. Rossell, M. F. Crommie, A. Zettl, *Nano Lett.,* 2008, **8**, 3582.

40 C. Quintana, J. M. Cowley, and C. Marhic, *J. Struct. Biol.,* 2004, **147**, 166.

41 B. Gu, X.-Q. Huang, S.-Q. Tan, M. Wang and W. Ji, *Appl Phys B*., 2009. **95**, 375.

42 X.-L. Zhang, Z.-B. Liu, X.-C. Li, Q. Ma, X.-D. Chen, J.-G. Tian, Y.-F. Xu and Y.-S. Chen, *Opt. Exp*., 2013**, 21**, 7511.

43 Z. Liu, Y. Wang, X. Zhang, Y. Xu, Y. Chen and J. Tian, *Appl. Phys. Lett*., 2009, **94**, 021902.

44 P. Pradhan, R. Podila, M. Molli , A. Kaniyoor, V. S. Muthukumar, S. S. S. Sai, S. Ramaprabhu and A.M. Rao, *Opt. Mater*., 2015, **39**, 182.

45 S.-Li. Guo, J. Yan, L. Xu, B. Gu, X.-Z. Fan, H.-T. Wang and N. B. Ming, *J. Pure. Appl. Opt. A*. 2002, **4 ,** 504.

46 D. I. Kovsh, D. J. Hagan and E. W. Van Stryland, *Opt. Exp*., 1999, **4**, 315.

47 Y. Fan, Z. Jiang and L. Yao, Chin. *Opt. Lett*., 2012, *10*, 071901.

48 M. B. M. Krishna, V. P. Kumar, N. Venkatramaiah, R. Venkatesan and D. N. Rao, *Appl. Phys. Lett*., 2011, **98**, 081106.

49 J. Zhu , Y. Li , Y. Chen , J. Wang , B. Zhang , J. Zhang and W. J. Blau, *Carbon*., 2011, **49**, 1900.

50 C. Zheng, W. Chen, Y. Huang, X. Xiao and X. Ye, *RSC Adv*., 2014**, 4**, 39697.

[Type text]

Graphical Abstract

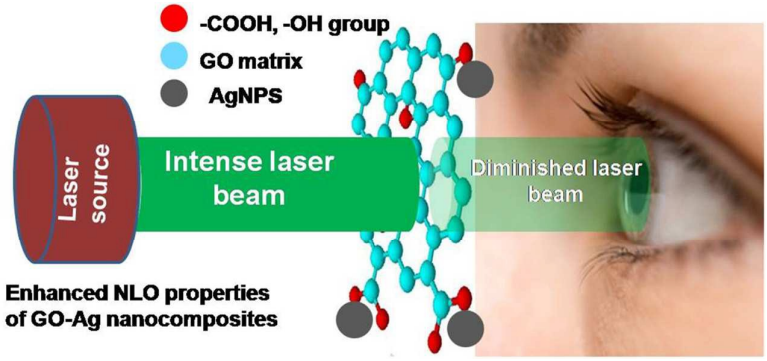

In this work, the synthesis of GO-Ag nanocomposite material has been reported and measured its nonlinear optical properties by the Z-scan technique at a visible wavelength of 532 nm. It is demonstrated that an enhancement (by a factor of ~ 2.8) in nonlinear optical properties of Go-Ag takes place, in comparison to that of GO due to the presence of Ag nanoparticles. Also it is found that the synthesized GO-Ag nanocomposite is exhibiting significant optical limiting effects.